Articles

Protein Interactions in the Human Methionine Synthase−Methionine Synthase Reductase Complex and Implications for the Mechanism of Enzyme Reactivation†

Kirsten R. Wolthers and Nigel S. Scrutton*

Faculty of Life Sciences, Manchester Interdisciplinary Biocentre, University of Manchester, 131 Princess Street, Manchester M1 7DN, United Kingdom

Received February 16, 2007; Revised Manuscript Received March 26, 2007

ABSTRACT: Methionine synthase (MS) is a cobalamin-dependent enzyme. It transfers a methyl group from methyltetrahydrofolate to homocysteine forming methionine and tetrahydrofolate. On the basis of sequence similarity with *Escherichia coli* cobalamin-dependent MS (MetH), human MS comprises four discrete functional modules that bind from the N- to C-terminus, respectively, homocysteine, methyltetrahydrofolate, cobalamin, and *S*-adenosylmethionine (AdoMet). The C-terminal activation domain also interacts with methionine synthase reductase (MSR), a NADPH-dependent diflavin oxidoreductase required for the reductive regeneration of catalytically inert cob(II)alamin (which is formed every 200−1000 catalytic cycles of MS) to cob(I)alamin. We have investigated complex formation between the (i) MS activation domain and MSR and (ii) MS activation domain and the isolated FMN-binding domain of MSR. We show that the MS activation domain interacts directly with the FMN-binding domain of MSR. Binding is weakened at high ionic strength, emphasizing the importance of electrostatic interactions at the protein−protein interface. Mutagenesis of conserved lysine residues (Lys1071 and Lys987) in the human activation domain weakens this protein interaction. Chemical cross-linking demonstrates complex formation mediated by acidic residues (FMN-binding domain) and basic residues (activation domain). The activation domain and isolated FMN-domain form a 1:1 complex, but a 1:2 complex is formed with activation domain and MSR. The midpoint reduction potentials of the FAD and FMN cofactors of MSR are not perturbed significantly on forming this complex, implying that electron transfer to cob(II)alamin is endergonic. The kinetics of electron transfer in MSR and the MSR−activation domain complex are similar. Our studies indicate (i) conserved binding determinants, but differences in protein stoichiometry, between human MS and bacterial MetH in complex formation with redox partners; (ii) a substantial endergonic barrier to electron transfer in the reactivation complex; and (iii) a lack of control on the thermodynamics and kinetics of electron transfer in MSR exerted by complex formation with activation domain. The structural and functional consequences of complex formation are discussed in light of the known crystal structure of human activation domain and the inferred conformational heterogeneity of the multidomain MSR−MS complex.

Methionine synthase (MS[1]) (EC 2.1.1.13) is an important enzyme for folate and homocysteine metabolism in mammals. The enzyme uses cob(I)alamin, a powerful nucleophile, to abstract a methyl group from CH_3-H_4folate to form methylcob(III)alamin and H_4-folate. The methyl group is subsequently transferred from methylcob(III)alamin to-homocysteine to form methionine and cob(I)alamin [eqs 1 and 2; (*1*)].

$$CH_3\text{-}H_4\text{folate} + \text{cob(I)alamin} \rightarrow H_4\text{-folate} + \text{methylcob(III)alamin} \quad (1)$$

$$\text{homocysteine} + \text{methylcob(III)alamin} \rightarrow \text{methionine} + \text{cob(I)alamin} \quad (2)$$

Occasionally (every 200−1000 catalytic cycles), cob(I)-alamin loses an electron, rendering MS inactive (*2*). In a unique reactivation mechanism, the inactive form (cob(II)-

† This work was funded by the UK Biotechnology and Biological Sciences Research Council. N.S.S. is a BBSRC Professorial Research Fellow.

* To whom correspondence should be addressed. Tel: +44 (0) 161 3065152. Fax: +44(0)1613068918. E-mail: nigel.scrutton@manchester.ac.uk.

[1] Abbreviations: MS, methionine synthase; MetH, *E. coli* cobalamin-dependent methionine synthase; hMS, human methionine synthase; MSR, methionine synthase reductase; AdoMet, *S*-adenosylmethionine; AdoHcy, *S*-adenosylhomocysteine; FMN, flavin mononucleotide; FAD, flavin adenine dinucleotide; NADPH, nicotinamide adenine dinucleotide phosphate; DTT, dithiothreitol; CH_3-H_4folate, methyltetrahydrofolate; H-folate, tetrahydrofolate; GST, glutathione-*S*-transferase; ox, oxidized; sq, semiquinone; hq, hydroquinone; CaM, calmodulin; NOS, nitric oxide synthase, CPR, cytochrome P450 reductase; NR1, novel reductase 1.

10.1021/bi700339v CCC: $37.00
Published on Web 05/04/2007

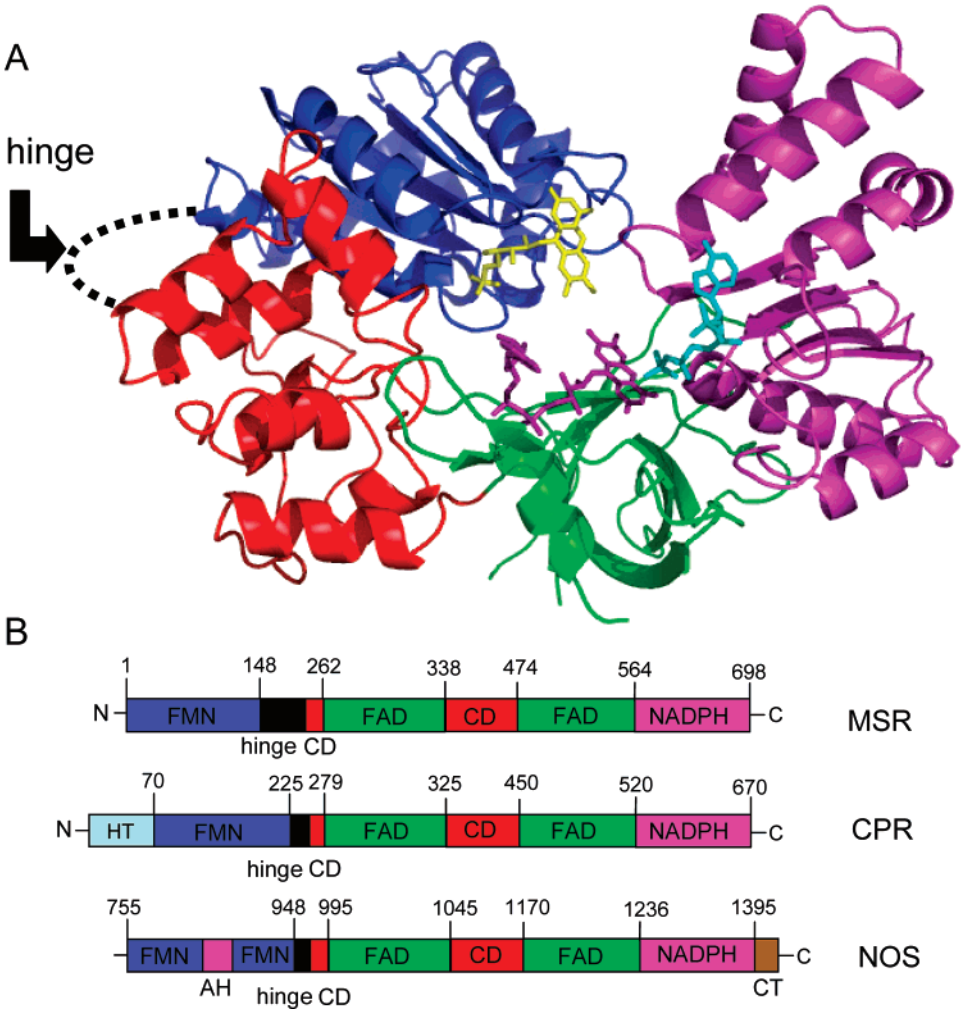

FIGURE 1: Molecular architecture of diflavin reductases. (Panel A) Ribbon diagram showing the structure of CPR, the prototype of the family. The FMN-domain is shown in blue, the connecting domain in red, the FAD domain in green, and the NADPH-binding domain in magenta. The cofactors are shown in ball and stick representation: FAD(purple), FMN (yellow), and $NADP^+$ (cyan). The hinge region (dashed loop) between the FMN-domain and the connecting domain is disordered in the CPR structure. (Panel B) Linear diagram comparing domain arrangement between MSR, CPR, and the reductase domain of NOS. Each cofactor binding domain is indicated and colored to match panel A. For CPR, HT refers to the N-terminal hydrophobic tail; for NOS, AH and CT denote the autoinhibitory helix and C-terminal domain, respectively. The connecting domain is abbreviated CD. The numbers above the box indicate approximate amino acid positions.

alamin) of the MS cofactor is reductively remethylated to form methylcob(III)alamin. In this reactivation mechanism, a complex is formed between MS and the diflavin oxidoreductase methionine synthase reductase (MSR), and electrons derived from the MSR-catalyzed oxidation of NADPH are transferred to the inactive from of MS (*3*, *4*). This long-range electron transfer in the MS−MSR complex facilitates methyl group transfer from AdoMet to MS [eq 3; (*5*)], thus generating methylcob(III)alamin, and MS is returned to the primary catalytic cycle.

$$S\text{-AdoMet} + \text{cob(II)alamin} + e^- \rightarrow S\text{-AdoHyc} + \text{methylcob(III)alamin} \quad (3)$$

Reactivation of the *E. coli* homologue of hMS, cobalamin-dependent methionine synthase (MetH), involves two independent flavoproteins, ferredoxin-$NADP^+$ oxidoreductase (FNR) and flavodoxin (Fld) (*6*). FNR is an FAD-containing enzyme that transfers electrons from NADPH to the FMN cofactor of flavodoxin. In the inactive state, MetH assembles with reduced Fld, and electron transfer to cob(II)alamin regenerates the active form of MetH (*7*).

The role of MS−MSR in human metabolism is multifaceted: MS recycles homocysteine, releases tetrahydrofolate, and produces methionine, a precursor for AdoMet biosynthesis. Impairment of MS or MSR activity can lead to high blood homocysteine levels, a condition linked to cardiovascular disease, neurological birth defects, and certain cancers, and a reduction in tetrahydrofolate pools, which impairs protein and DNA synthesis and ultimately cell division (*8*−*11*). The primary structure of human MSR (78 kDa) reveals two distinct flavin-binding domains, an architecture typical of the diflavin reductase family. Mammalian enzymes that belong to this family include the nitric oxide synthases [NOS; (*12*, *13*)] human novel oxidoreductase 1 [NR1; (*14*)] and cytochrome P450 reductase [CPR; (*15*)]. These enzymes contain an N-terminal NADPH/FAD-binding domain (related to FNR), a connecting domain, and a C-terminal flavodoxin-like FMN-binding domain (Figure 1). In addition, there is a linker tethering the connecting domain with the FMN-domain which is extended by a further 90 residues in MSR. This extended linker might confer relative mobility of the flavin-

binding domains in MSR, and thus have a role in formation of the MS−MSR complex.

Fld forms mutually exclusive complexes with FNR and MetH and interacts with FNR and MetH using the same surface region of Fld (*16*). Thus, formation of a ternary complex between all three proteins is not possible. A similar mode of recognition in the human system would require movement of the FMN-domain between the NADPH/FAD-domain of MSR and MS while being tethered to the FAD-domain by the extended connecting domain. A similar mechanism has been suggested for neuronal nitric oxide synthase (nNOS) to shuttle electrons between the NADPH/FAD-domain and heme-dependent oxygenase domain (*17*).

Determination of the crystal structure of human MS activation domain represents an important step in understanding the mechanism of electron transfer in the human MS−MSR complex. Although the structure of human activation domain closely resembles the activation domain of MetH (*18*), there are (minor) structural differences centered around residue Lys987 (*19*). The corresponding residue (Lys959) in MetH is implicated in complex formation with Fld by forming a salt bridge with residue Glu61 of Fld (*20*). The observed structural differences between the MetH and human activation domains suggest a different mode of interaction with their cognate redox partners. Partner interactions are specific: MSR cannot reactivate MetH, and *E. coli* FNR/FLD cannot substitute for MSR in the reactivation of human MS (*21*).

We have demonstrated major differences in the thermodynamic driving force for electron transfer in MSR compared with the *E. coli* system (*22*). The midpoint potentials of the $FMN_{ox/sq}$ (−260 mV) and $FMN_{sq/hq}$ (−440 mV) of Fld (*23*) are substantially more electronegative than the corresponding couples in MSR [$FMN_{ox/sq}$ = −109 mV, and $FMN_{sq/hq}$ = −227 mV; (*22*)]. If the potential of the cob(II)alamin/cob(I)alamin in human MS is similar to that reported for MetH [−490 mV; (*23*)], there is a substantial thermodynamically unfavorable barrier for electron transfer from MSR to MS. Perturbation of the MSR redox potentials in the MS−MSR complex might provide a solution to the presence of this endergonic barrier in the uncomplexed partner proteins. The rearrangement of residues close to flavin cofactors is known to influence the reduction potentials of other flavoproteins (*24*).

In this article, we have investigated structural determinants and functional consequences of complex formation in the human MS−MSR complex. We highlight some similarities and also the major differences in the reactivation complexes of the human and *E. coli* systems. We show that complex formation does not perturb the thermodynamic driving force or the kinetics of electron transfer in human MSR, supporting the view that the reactivation chemistry involves a major endergonic electron transfer step, absent in the *E. coli* system, on conversion of cob(II)alamin to cob(I)alamin. We demonstrate a role for electrostatic stabilization of the human MSR−MS complex and different complex stoichiometries with full-length MSR and the isolated FMN-domain of MSR. Our data are discussed in light of the recent structural determination of the activation domain for human MS (*19*).

EXPERIMENTAL PROCEDURES

Materials. Restriction enzymes were supplied by New England Biolabs. Competent *E. coli* XL1 Blue cells and *Pfu* Turbo DNA polymerase were supplied by Stratagene. Complete protease inhibitor tablets were from Roche. All other reagents were from Sigma Chemical Company.

Preparation of Proteins. The recombinant form of the hMS activation domain was purified as previously described (*19*). Full-length MSR and the component activation domain were expressed and purified with a minor modification to the published protocol (*22*). The procedure for purifying MSR and the individual flavin domains was adapted from literature supplied by Novagen. The cell pellet was resuspended in buffer A (4.3 mM Na_2HPO_4, 1.47 mM KH_2PO_4, 0.137 M NaCl, 2.7 mM KCl at pH 7.3, 1 mM EDTA, and 1 mM DTT) supplemented with complete protease inhibitor tablets. The cells were lysed by the addition of 200 μg/mL lysozyme and by sonication (8 × 20 s pulses at 25% power with 3 min intervals using a Bandelin sonoplus GM2600). The lysate was centrifuged at 15,000*g* for 50 min, and the supernatant was loaded onto a glutathione-Sepharose 4B column (75 × 39 mm) equilibrated with buffer A. The column was washed with 3 L of buffer A. The chimeric protein, GST-MSR, was eluted with buffer B (50 mM Tris-HCl at pH 7.5, 1 mM DTT, 1 mM EDTA, and 10 mM glutathione). The GST-tag was cleaved from MSR by incubation with thrombin at 4 °C. MSR was dialyzed (16 h) against buffer A to remove glutathione. The cleaved MSR was reapplied to a glutathione-Sepharose 4B column (54 × 30 mm) equilibrated with buffer A. MSR was separated from the remaining glutathione-binding proteins by washing the column with buffer A. MSR was dialyzed (16 h) against 50 mM Tris HCl at pH 7.5 and 4 °C. The protein was purified further by anion-exchange chromatography on a Q-Sepharose high-performance column (145 × 25 mm) and eluted using a linear gradient ranging from 0 to 0.5 M NaCl in 50 mM Tris-HCl, pH 7.5; at a flow rate of 4 mL/min. The MSR fractions, as indicated by absorbance at 450 and 275 nm, were collected and concentrated by ultrafiltration. The protein was dialyzed against 50 mM Tris-HCl buffer at pH 7.5, containing 50% glycerol, and stored at −80 °C. The FMN-domain was expressed, purified, and stored using the same purification protocol. The concentration of MSR and the FMN-domain was determined by absorbance values at 450 nm with molar extinction coefficients of 25,600 and 14,700 M^{-1} cm^{-1}, respectively.

Mutagenesis of Putative Interface Residues of Human MS and MSR. The QuikChange protocol was employed (Stratagene) to create site-directed mutants of the MS activation domain and the MSR FMN-domain. The complementary primers, 5′-CTA CCA CGG GCA CCG GAG CCC CAC CCG ACA CAG CC-3′ and 5′-GGC TGT GTC GGG TGG GGC TCC GGT GCC CGT GGT AG-3′, were used to generate the D65A mutation in pGEXFMNH (*22*), the expression construct for the FMN-domain. The forward and reverse primers, 5′-TGG CAG CTC CGG GGC ACG TAC CCG AAT CGA GGC-3′ and 5′-GCC TCG ATT CGG GTA CGT GCC CCG GAG CTG CCA G-3′, were employed for generating the K987T mutation in pETACT (expression plasmid for the MS activation domain) (*19*), while the K1071T mutation in the same plasmid was produced with

the following complementary primers: 5′-GGC AAC AGG CTG AGA CGG ACT CTG CCA GCA CG-3′ and 5′-CGT GCT GGC AGA GTC CGT CTC AGC CTG TTG CC-3′. The mutant plasmids were sequenced (MWG Biotech, London) to ensure that no other base changes had occurred. The plasmids encoding the FMN-domain and the MS activation domain mutant proteins were transformed into *E. coli* strain BL21(DE3), and the recombinant proteins were expressed and purified as for wild type proteins.

Chemical Cross-Linking. To cross-link the MSR FMN-domain and MS activation domain, the reagents 1-ethyl-3-[3-(dimethylamino)propyl]carbodiimide (EDC) and sulfo-*N*-hydroxysuccinimide (NHC) were employed in a two-step reaction at room temperature. The FMN-domain (25 μM) and the activation domain (25 μM) were incubated separately for 5 min with 5 mM EDC and 5 mM sulfo-NHS in 20 mM 2-*N*-(morpholino)ethanesulfonic acid buffer at pH 6.0. The reaction was quenched by the addition of 20 mM 2-mercaptoethanol, and then the partner protein was added to the sample. After 2 h, the reaction was terminated by the addition of 10 mM *N*-hydroxylamine, which regenerates those acidic residues that had been converted to the succinimidyl ester intermediate with EDC and sulfo-NHS but were unable to cross-link. Samples were then analyzed by SDS−PAGE gel electrophoresis using 12% SDS−polyacrylamide gels.

Fluorescence Measurements. Fluorescence quenching experiments were performed in 50 mM Tris-HCl at pH 7.5 and 25 °C in a 3 mL volume using a Cary Eclipse Fluorescence Spectrophotometer (Varian). The FMN-domain (0.25 μM) was excited at 450 nm (the absorbance maximum of the flavin cofactor), and emission spectra were recorded between 500 and 600 nm. Excitation and emission slit widths were 10 and 5 nm, respectively. After addition of activation domain (1−8 μL samples from a concentrated protein stock solution), the sample was mixed and incubated for 1 min before emission spectra were recorded. The change in fluorescence of the emission maximum (529 nm) was plotted against the concentration of the activation domain and the data were fit to eq 4

$$\Delta F = F_0 + 2\Delta F_{max}(E_0 + L + K_d) - \sqrt{(E_0 + L + K_d)^2 - 4E_0L} \quad (4)$$

where ΔF represents the change in fluorescence intensity, F_0 is the fluorescence intensity in the absence of the activation domain, E_0 is the concentration of the FMN-domain, L denotes the concentration of the activation domain added to the sample, and K_d represents the dissociation constant. Fluorescence binding assays involving the mutant forms of the FMN-domain and the activation domain employed the same protocol, and data were analyzed by the same method. The dependence of ionic strength on binding affinity was determined in 50 mM Tris-HCl at pH 7.5, to which a variable amount of KCl was added.

Isothermal Titration Calorimetry. Isothermal titration calorimetry (ITC) was performed using a VP-ITC microcalorimeter (Microcal Inc.). Protein samples were exchanged into 50 mM Tris HCl at pH 7.5 by dialysis. The concentration of the activation domain was determined using the Bradford assay with BSA as the standard. Titrations were performed at 25 °C, and protein solutions were degassed by vacuum aspiration for 8 min at 23 °C prior to loading the samples in the ITC cell and syringe. Aliquots (10 μL) of MSR or the isolated FMN-domain at concentrations of 0.9−1.1 mM were titrated into 1.28 mL of 120−190 μM MS activation domain at 360 s intervals with a stirring speed of 350 rpm. Parallel experiments were performed by injecting the FMN-domain and MSR into buffer or the buffer into the activation domain to determine heats of dilution. The heats of dilution were negligible and subtracted from their respective titrations prior to data analysis. Thermodynamic parameters, n (stoichiometry), K_d ($1/K_A$ the association constant), and $\Delta H°$ (enthalpy change), were obtained by nonlinear least-squares fitting of experimental data using the single-site binding model of the Origin software package (version 5.0) provided with the instrument. The free energy of binding ($\Delta G°$) and entropy change ($\Delta S°$) were obtained using the following equations.

$$\Delta G° = -RT \ln K_A \quad (5)$$

$$\Delta G° = \Delta H° - T\Delta S° \quad (6)$$

Spectroelectrochemical Redox Potentiometry. Redox titrations were performed in a Belle Technology glove box under a dinitrogen atmosphere, maintained at less than 5 ppm oxygen. The buffer solution used (50 mM Tris-HCl buffer at pH 7.5) was extensively bubbled with nitrogen and then introduced to the glove box and allowed to equilibrate with the oxygen-free atmosphere for 16 h. A concentrated (0.3−0.5 mM) 1−2 mL sample of protein (MSR or FMN-domain) was transferred into the glove box and applied to a Pharmacia PD-10 desalting column equilibrated with the anaerobic buffer to remove oxygen. The eluted protein (FMN-domain or MSR) was diluted to 8 mL with the anaerobic titration buffer (50 mM Tris-HCl buffer at pH 7.5) to a final concentration of ∼30 μM. Anaerobic solutions of the activation domain were obtained similarly and were added at a concentration of 50 μM to the flavoprotein sample, where appropriate. The following mediators were added to the 8 mL protein samples to facilitate electron exchange between enzyme and electrode: 2 μM phenazine methosulfate, 5 μM 2-hydroxy-1,4-naphthoquinone, 0.5 μM methyl viologen, and 1 μM benzyl viologen. Protein solutions were reduced slowly with 0.5−1 μL aliquots of sodium dithionite taken from concentrated stock solutions (typically 10−50 mM). After each addition of reductant, the absorbance spectrum (300−800 nm) was recorded using a Cary UV-50 Bio UV−visible scanning spectrophotometer. Following attainment of equilibrium, the electrochemical potential of the solution was measured using a Hanna pH 211 meter coupled to a Pt/Calomel electrode (ThermoRussell, Ltd.) at 25 ± 2 °C. The electrode was calibrated using the Fe^{3+}/Fe^{2+} EDTA couple as a standard (+108 mV). A factor of +244 mV was used to correct relative to the standard hydrogen electrode.

The redox potential of $FMN_{ox/sq}$ and $FMN_{sq/hq}$ couples of the isolated FMN-domain were determined by plotting the absorbance values at 454 and 600 nm, the near absorbance maxima for the fully oxidized flavin and blue neutral semiquinone, against the recorded potential (*22*). The data were fit by nonlinear least-squares regression analysis to eq 7, which is derived by extension of the Beer−Lambert law and the Nernst equation and describes a two-electron reduction process.

$$A = \frac{a10^{(E - E'_1)/59} + b + c10^{(E'_2 - E)/59}}{1 + 10^{(E - E'_1)/59} + 10^{(E'_2 - E)/59}} \quad (7)$$

In eq 7, A is the total absorbance; a, b, and c are component absorbance values contributed by a flavin in the oxidized, semiquinone, and reduced states, respectively. E is the observed potential; E_1', and E_2', are the midpoint potentials for oxidized/semiquinone and semiquinone/hydroquinone couples, respectively.

Determination of the four midpoint potentials in full-length MSR relied on absorbance values at 425 and 501 nm, which are isosbestic points shown in the spectral titration of MSR. The absorbance at 501 nm (apparent isosbestic point for the FAD and FMN oxidized/semiquinone couples) and 425 nm (isosbestic for the FAD and FMN semiquinone/hydroquinone couples) were plotted versus the potential, and the data were fit to eq 7 to obtain approximations of the opposite redox couples. Optical potentiometry experiments with MSR were also analyzed by global analysis using SpecFit/32 (Bio-Logic Science Instruments, Grenoble, France). The spectra were deconvoluted, and the potentials were determined using a Nernstian model with five species and four $n = 1$ potentials: $a \leftrightarrow b \leftrightarrow c \leftrightarrow d \leftrightarrow e$.

Stopped-Flow Kinetic Measurements. Stopped-flow studies were performed using an Applied Photophysics SX.17 MV stopped-flow spectrophotometer. Experiments were performed under anaerobic conditions at 25 °C in 50 mM Tris-HCl buffer at pH 7.5, and the protein concentration was 13 μM (reaction cell concentration). The sample handling unit of the stopped-flow instrument was contained within a glove box (Belle Technology), and the buffer was made anaerobic by extensive bubbling with nitrogen before use. Prior to stopped-flow studies, 2 mL of MSR was treated with potassium ferricyanide, and excess ferricyanide and oxygen were removed by rapid gel filtration in the glove box using an Econo-Pac 10 DG column (Bio-Rad) equilibrated in anaerobic 50 mM Tris-HCl buffer at pH 7.5. The activation domain was made anaerobic by the same procedure and added to the MSR sample where appropriate (final reaction cell concentration of 40 μM). Stopped-flow multiwavelength absorption studies were carried out using a photodiode array detector and X-SCAN software (Applied Photophysics Ltd., Surrey, U.K.). Spectral deconvolution was performed by singular-value decomposition (SVD) methods using PROKIN software (Applied Photophysics Ltd.).

RESULTS

Fluorescence Binding Assays. The binding affinity of the activation domain for the isolated FMN-binding domain was determined through fluorescence titration assays. The flavin cofactor was excited near its absorption maximum (450 nm), and the change in the emission spectrum was monitored between 500 and 600 nm. Addition of the activation domain to the FMN-domain resulted in a quenching of the intrinsic flavin fluorescence, suggesting that the flavin chromophore is shielded from the solvent in the protein−protein complex. The decrease in the intensity of the fluorescence emission spectra shows a hyperbolic dependence on the concentration of the activation domain (Figure 2). A fit of eq 4 to the data yielded the apparent dissociation constant (K_d of 1.5 μM) for binding of the activation domain to the FMN-binding region of MSR (Table 1). Electrostatic interactions on the surface of the protein are likely to be important in complex formation, as an increase in ionic strength results in a decrease in binding affinity (Table 1).

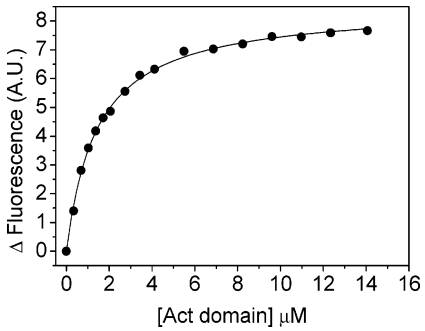

FIGURE 2: Fluorescence titration of the FMN-domain with the MS activation domain. The FMN-domain (0.25 μM) was titrated with activation domain under the conditions described in Experimental Procedures. The change in flavin fluorescence intensity at 529 nm was plotted versus the concentration of the activation domain, and the curve shows the best fit of the data to eq 4. Table 1 lists the calculated dissociation constants for the FMN-domain−activation domain complex at different ionic strengths.

Table 1: Effects of Ionic Strength and Single Mutations on the Dissociation Constant for the Activation Domain−FMN-Domain Complex

enzyme	salt concentration	K_d (μM)
Act-domain wild-type	0 mM KCl[b]	1.5 ± 0.1
	60 mM KCl[b]	10.9 ± 1.1
	150 mM KCl[b]	36.0 ± 1.9
	300 mM KCl[b]	43.2 ± 8.0
Act-domain K987T[a]		8.9 ± 0.8
Act-domain K1071T[a]		29.2 ± 2.6
FMN-domain M22I[a]		1.7 ± 0.1
FMN-domain D65A[a]		1.8 ± 0.2

[a] Titration was performed in 50 mM Tris-HCl at pH 7.5, as described in Experimental Procedures. [b] Titration was performed with the wild type activation domain as described in Experimental Procedures.

Chemical Cross-Linking of Activation Domain and FMN-Domain. To verify that the observed quenching of fluorescence emission spectra is a result of protein−protein interaction, an attempt was made to covalently link the activation domain to the FMN-binding domain using cross-linking reagents. The structures of *E. coli* flavodoxin (*25*) and the FMN-domains of NOS (*17*) and CPR (*15*) reveal a number of surface-exposed acidic residues, which are known to be important for protein contact with physiological electron acceptors. The corresponding partner protein contains a cluster of basic residues that enable salt bridges to be formed between the two partner proteins. To establish if this electrostatic relationship is conserved in MS and MSR, EDC and sulfo-NHS were used as cross-linking reagents. These cross-linking reagents have been employed successfully in cross-linking studies of the interaction of Fld with FNR, MetH, and the MetH activation domain (*20*). The carbodiimide of EDC reacts specifically with acidic residues to produce an unstable amine-reactive species. Sulfo-NHS reacts with this species to form a more stable succinimidyl ester, thereby increasing the amount of cross-linked species. Thus, EDC and sulfo-NHS were added to the FMN-domain or the activation domain to activate surface exposed acidic residues. Following a short incubation period, the partner protein was then added to the solution. If the activated acidic

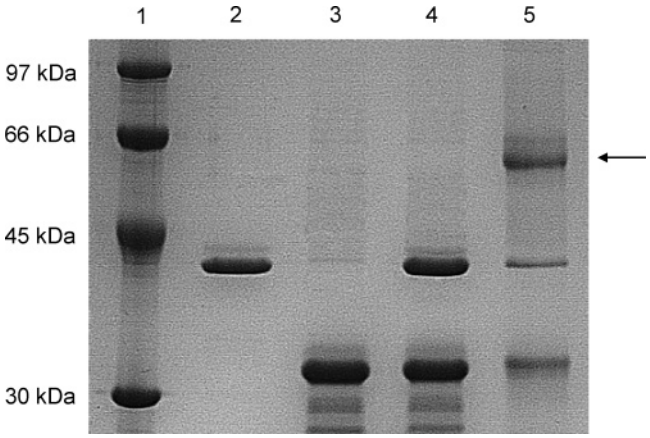

FIGURE 3: Analysis of cross-linking the FMN-domain and the hMS activation domain. Acidic residues on one protein were activated with 5 mM EDC and 5 mM NHS for 5 min. Activation was quenched, and the second protein was added and incubated for 2 h. Samples were analyzed by SDS−PAGE. Lane 1, molecular weight markers; lanes 2 and 3, purified FMN domain and the hMS activation domain, respectively; lane 4, acidic residues on hMS activated and followed by the addition of FMN-domain (no cross linked complex observed); lane 5, acidic residues on the FMN-domain activated for cross-linking followed by addition of the hMS activation domain. The cross-linked complex between the FMN domain and hMS activation domain is shown by the arrow.

residue of one protein is in close proximity to a basic residue of the partner protein, the formation of an isopeptide bond and cross-linked species is expected.

Treatment of the 32 kDa FMN-domain with EDC and sulfo-NHS followed by the addition of the activation domain results in the formation of a protein species of higher apparent molecular weight, consistent with the presence of a cross-linked complex between the activation domain and the FMN-domain (Figure 3, lane 5). Analysis by mass spectrometry of the trypsin-digested higher molecular weight species revealed that this material comprised the activation and FMN-domains. Reaction of the activation domain with EDC and sulfo-NHS followed by subsequent addition of the FMN-domain does not yield a cross-linked protein. These observations are consistent with the presence of acidic residues on the surface of the FMN-domain that interact electrostatically with basic residues found on the surface of the activation domain during complex assembly.

Effects of Surface Mutations on Binding Affinity. Succinimidyl esters are essentially specific for lysine residues, and surface lysines were therefore considered to be the only basic amino acids involved in cross-linking the activation domain and the FMN-binding domain. Two lysine residues (K959 and K1035) in MetH are known to contact Fld, as mutation of these residues to threonine resulted in a significant decrease in the binding affinity of this flavoprotein for partner proteins (*20*). The corresponding residues are conserved in MS (K987 and K1071); however, the crystal structure of the hMS activation domain reveals a significant structural difference around K987 (*19*), which is an exposed residue close to the Ado-Met binding region. We have mutated K987 and K1071 to threonine to investigate the importance of these residues in forming the complex interface with the FMN-binding domain of MSR.

Both mutant human activation domains (K987T and K1071T) were titrated against the FMN-domain and the fluorescence emission maximum recorded. As for the wild type activation domain, the fluorescence emission intensity displayed a hyperbolic dependence on the concentration of the K1071T and K987T proteins. A fit of eq 4 to the data revealed a dissociation constant of 7.8 μM for K987T and 29 μM for the K1071T activation domains, which are significantly higher (6-fold and 25-fold, respectively) than the value measured for wild type activation domain (Table 1). This implies that electrostatic interactions are important in stabilizing the complex formed between the FMN-domain and the activation domain.

The dissociation constant (1.8 μM) for the complex formed with the D64A mutant of the MSR FMN-domain and activation domain is similar to that measured for the wild type complex (Table 1). Also, we were able to chemically cross-link the D64A FMN-domain mutant with the activation domain (data not shown), suggesting that this residue is not a key binding determinant in the MSR−MS complex. In the Supporting Information (Figure S1), we have compared the electrostatic surface potential for Fld (in the region of the solvent exposed FMN) with that of a homology model of the MSR FMN-domain (based on the structure of Fld). The surface corresponding to the putative location for interaction with MS and/or the MSR NADPH/FAD-binding region is less negatively charged compared to the corresponding region of Fld. Nevertheless, there are several acidic residues close to Asp64 and the FMN that are potential cross-linking candidates, and work is underway to determine the specific residue(s) involved in the interaction, a task that is hampered by the lack of a structure for the MSR FMN-domain. The retention of common binding residues between the *E. coli* and human MS activation domains is perhaps expected given the high level of sequence identity (55%). That the D64A mutant FMN-domain did not mimic the properties of the corresponding Fld mutant might reflect the lower degree of sequence identity (22%) between these proteins.

We have investigated the binding of a polymorphic variant of MSR, M22I, localized to the FMN-domain using the fluorescence binding assay. Individuals with this variation exhibit mild hyperhomocysteinemia, a risk factor for cardiovascular disease (*26*), and a maternal risk factor for children with a craniofacial anomaly, Down's syndrome or neural tube defects (*27*). The variant activates MS with the same maximal velocity, but a 3−4-fold higher ratio of MSR to MS is required to elicit the same maximal activity as that of the wild type (*28*). We have demonstrated that the midpoint potentials and rates of hydride transfer and internal

Table 2: Thermodynamic Parameters for the Binding of MSR and the FMN-Domain Binding to the MS Activation Domain, as Determined by Isothermal Titration Calorimetry

	K_d (μM)	n	$\Delta H°$ (kJ/mol)	$\Delta G°$ (kJ/mol)	$\Delta S°$ (J mol^{-1} K^{-1})
FMN-domain	1.8 ± 0.3	0.97 ± 0.01	−36.14 ± 0.47	−32.75 ± 0.35	−11 ± 2
MSR	4.5 ± 0.4	0.51 ± 0.02	−130.16 ± 2.25	−30.51 ± 0.21	−334 ± 8

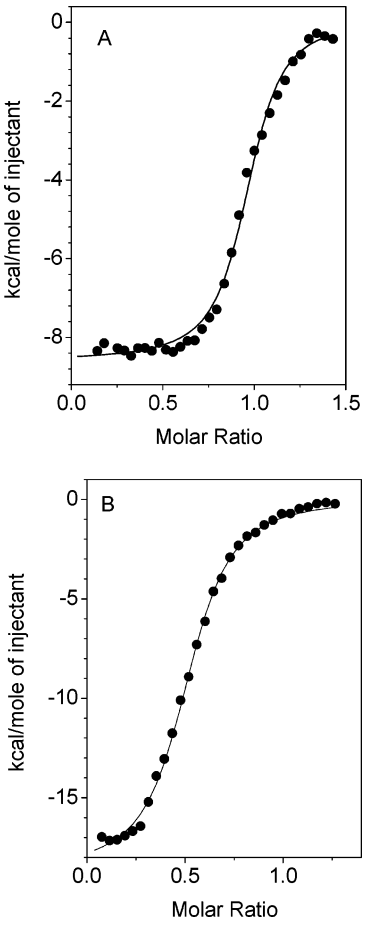

FIGURE 4: Isothermal titration calorimetry of the activation domain with the FMN-domain and MSR. All titrations were performed in 50 mM Tris-HCl at pH 7.5 at 25 °C. The points are fit to a one-site model. (Panel A) Titration of activation domain with FMN-domain. The stock concentration of FMN-domain is 1.15 mM, and repeated injections of 10 μL were added to the activation domain. The concentration of the activation domain is 193 μM. (Panel B) Titration of activation domain with MSR. The stock concentration of MSR is 0.94 mM, and repeated injections of 10 μL were added to the activation domain. The concentration of the activation domain is 150 μM. The thermodynamic binding parameters, ($\Delta S°$, $\Delta G°$, $\Delta H°$, and K_d) for both binding isotherms are listed in Table 2.

electron transfer are the same in this polymorphic variant compared to the wild type (*29*), leading us to inquire if the M22I mutation affects the stability of the MS−MSR complex. Fluorescence binding assays show, however, that the complex dissociation constant for the M22I FMN-domain−activation domain complex (1.8 μM) is similar to that measured for wild type FMN-domain (Table 1). The origin of the apparent defect that causes mild hyperhomocysteinemia thus remains uncertain.

Isothermal Calorimetry. We have investigated the thermodynamic parameters associated with the binding of full-length MSR and the FMN-domain to the MS activation domain using ITC. The dissociation constant for the component FMN-domain measured by ITC (1.8 μM; Table 2) is similar to that determined using the fluorescence assay. The dissociation constant for MSR (4.5 μM) is 2.5-fold higher than that of the isolated FMN-domain. For both MSR and the FMN-domain, the binding isotherm was exothermic and not entropically driven (Table 2; Figure 4). The change in enthalpy ($\Delta H°$) for binding was 3.6-fold greater with full-length MSR (−130 kJ/mol) compared to that with the FMN-domain (−36 kJ/mol). The increase in binding enthalpy suggests that MSR might undergo additional conformational changes upon interaction with the activation domain and that the decrease in entropy may be associated with conformational restrictions of the protein in the complex. The calculated binding stoichiometry (n) is ∼1 for the binding of the activation domain to the FMN-domain and ∼0.5 for the binding of MSR to the activation domain. The data are consistent with the formation of a 1:1 complex between the activation domain and the FMN-domain. With full-length MSR, however, the observed stoichiometry is inconsistent with the formation of a 1:1 complex. In this case, either (i) two molecules of activation domain (or a dimer of the protein) interact with one molecule of MSR or (ii) a subpopulation of MSR only interacts with the activation domain. Given that the activation domain exists as a monomer−dimer equilibrium (*19*), albeit favoring formation of the monomeric species, the former is perhaps more plausible, with the equilibrium position being shifted toward the dimer through complex formation with MSR.

Effects of the Activation Domain on the Midpoint Reduction Potentials of the Flavin Cofactors in MSR. We have previously measured the midpoint reduction potentials for the four flavin couples in MSR (*22*). In extending this study, we have measured these potentials in the MSR−activation domain complex to address the possibility that complex formation (partially) overcomes the large thermodynamic barrier for electron transfer to the cob(II)alamin cofactor. The midpoint potentials of the flavin cofactors in MSR and the component FMN-domain were measured in the presence of the activation domain to determine if complex formation perturbs the redox properties of the flavin cofactors. Figure 5A shows the spectral changes during redox titration of the FMN-domain. The addition of dithionite to the oxidized flavoprotein results in a decrease in absorbance at 454 nm and a concomitant increase in absorbance at 594 nm (solid line) as fully oxidized cofactor converts into the blue neutral semiquinone species (FMN_{sq}). Further reduction, by a second reducing equivalent, leads to a loss in absorbance at 454 and 594 nm as the blue semiquinone is converted to the FMN hydroquinone. A plot of the absorbance values at 600 nm versus the recorded potential produced a bell-shaped curve, reflecting the appearance and disappearance of the blue FMN semiquinone (Figure 5B). In contrast, a sigmoidal shaped curve is obtained in a plot of the absorbance values at 454 nm versus the recorded potential (Figure 5C). A fit of the data in Figure 5B and C to eq 7 yields midpoint potentials for the $FMN_{ox/sq}$ and $FMN_{sq/hq}$ couples of −94 and −192 mV (Figure 5B) and −96 and −208 mV (Figure 5C), respectively. The presence of the activation domain in the redox titrations does not appear to substantially affect the thermodynamics of flavin reduction. A fit of the data in Figure 5B and C to eq 7 yields potentials for the $FMN_{ox/sq}$ (−86 mV; −83 mV) and $FMN_{sq/hq}$ (−170 mV; −180 mV), which are close to the values obtained in the absence of the activation domain (Table 3).

The midpoint potentials of all four redox couples ($FMN_{ox/sq}$, $FMN_{sq/hq}$, $FAD_{ox/sq}$, and $FAD_{sq/hq}$) in full-length MSR were also measured in the presence and absence of the activation domain. Reduction of fully oxidized MSR, leads to an initial decrease in absorbance at 454 nm with a concomitant increase in absorbance at 595 nm (solid lines in Figure 6A).

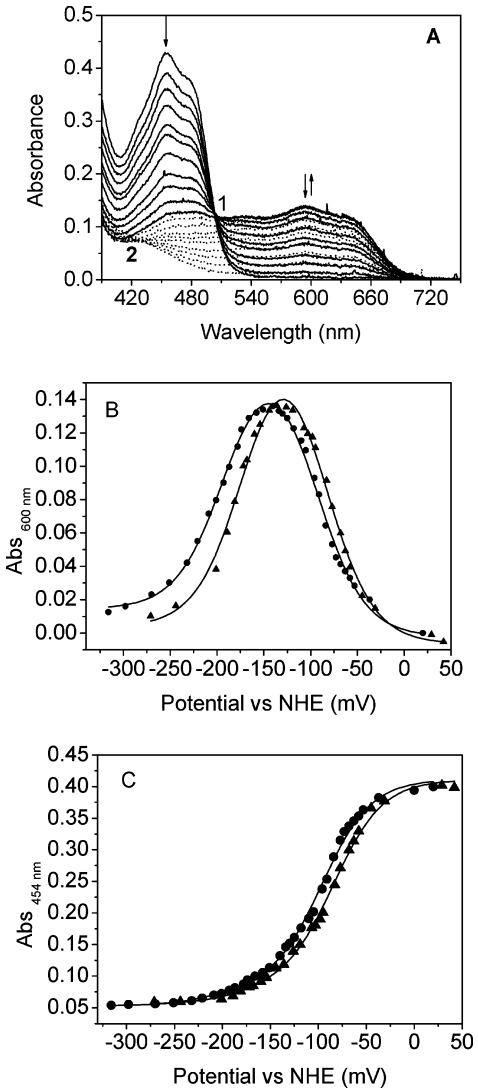

FIGURE 5: UV−visible absorption spectra collected during spectroelectrochemical titrations of the FMN-domain. FMN-domain concentration is 30 μM. (Panel A) Arrows indicate direction of absorption change at key wavelengths during the reductive phase of the redox titrations, and the solid lines demark spectra recorded during the addition of the first electron (i.e., conversion of the FMN oxidized to the semiquinone state). An isosbestic point appearing at 501 nm is indicated by "1". The dotted lines are spectra taken during the addition of the second reducing equivalent and show the flavin semiquinone to hydroquinone transition. A second isosbestic point, denoted by "2", appears in this phase at 425 nm. (Panels B and C) Plots of absorbance at 600 and 454 nm vs potential for the FMN-domain of MSR with (▲) and without (●) the activation domain (40 μM), respectively. The data were fitted to eq 7, and the resultant values for the redox potentials for the ox/sq and sq/hq couples for FMN are shown in Table 3. Anaerobic titrations were performed in 50 mM Tris-HCl buffer at pH 7.5 and 25 °C, and methods are described in Experimental Procedures.

During this phase of the titration, an isosbestic point is present at 501 nm. Upon further addition of the reductant, the semiquinone signal at 594 nm remains close to its maximal absorbance, while the absorbance values at shorter wavelengths decrease (dashed lines in Figure 6A). Isosbestic points are absent during this phase of the titration as multiple partially reduced forms of MSR exist, which are inferred to be the FMN_{sq}/FAD_{ox}, FMN_{sq}/FAD_{sq}, and FMN_{hq}/FAD_{sq} forms. In the third and final phase of the redox titration (dotted lines in Figure 6A), at potentials more negative than −250 mV, the semiquinone signal decreases concomitantly with a further decrease in absorbance at 450 nm. A second isosbestic point appears during this phase at 425 nm, reflecting the transition of FAD_{sq} to FAD_{hq}.

Redox titration data for full-length MSR were analyzed by plotting the isosbestic points at 501 and 425 nm versus the measured potential (Figure 6B and C, respectively). At an isosbestic point, there is a near-zero absorbance change occurring with the electronic transition of a redox couple, the ox/sq transition in the case of the isosbestic point at 501 nm. Thus, a plot of absorbance change at 501 nm versus potential can be used to determine the midpoint potentials of the sq/hq couples for each of the flavins. Conversely, a plot of absorbance at 425 nm versus potential can be used to determine the midpoint potentials of the ox/sq couples for each of the flavins. The data shown in Figure 6B and C were fitted to eq 7. The calculated midpoint potentials of the four couples are $FMN_{ox/sq} = -86$ mV; $FMN_{sq/hq} = -183$ mV; $FAD_{ox/sq} = -255$ mV; and $FAD_{sq/hq} = -285$ mV (Table 3). In the presence of the activation domain, the redox couples are $FMN_{ox/sq} = -77$ mV; $FMN_{sq/hq} = -183$ mV; $FAD_{ox/sq} = -262$ mV; and $FAD_{sq/hq} = -289$ mV (Table 3). Thus, the presence of the activation domain does not significantly perturb the thermodynamic properties of the flavin cofactors in full-length MSR.

We also analyzed redox titration data by global fitting of the UV−visible data. The entire spectral data from 300 to 800 nm throughout the redox titration were processed by singular value decomposition to deconvolute the spectra of each reduced species. Analysis of the processed data revealed five spectral species (Figure 6D). The data were globally analyzed using a Nernstian model with five species and four $n = 1$ potentials: $a \leftrightarrow b \leftrightarrow c \leftrightarrow d \leftrightarrow e$. The four potential values, listed in Table 3, show a good correlation with the midpoint potentials calculated using the Nernst equation at single wavelengths. The only exception is the $FAD_{sq/hq}$ couple, which is ~30 mV lower when the data are analyzed using global fitting compared with fits of the data using the appropriate Nernst equations. This discrepancy might result from potential difficulties in deconvoluting the spectra of the fully reduced (4 electron) species. Global analyses of the data indicate that the presence of the activation domain does not alter the thermodynamic properties of MSR.

Influence of the Activation Domain on the Kinetics of MSR Flavin Reduction. We investigated potential effects of activation domain binding to MSR on the rate of hydride transfer and/or interflavin electron transfer using stopped-flow mixing and spectrophotometry. The methods are similar to those we have used in stopped-flow studies of flavin reduction in MSR in the absence of partner proteins (*30*). Thus, MSR (13 μM; syringe concentration) in the absence or presence of the activation domain (40 μM; syringe concentration) was rapidly mixed with NADPH (200 μM; syringe concentration) under pseudo-first-order conditions in an anaerobic environment at 25 °C. Following rapid mixing of MSR with NADPH, absorbance spectra (300−800 nm) were collected over 500 s. Complete bleaching of the absorbance maximum at 454 nm was observed, signifying reduction of MSR to the 4 electron level (Figure 7A). The spectral data over 500 s were processed by singular value decomposition using PROKIN software and were best fit to a three-step reversible kinetic model (A ↔ B ↔ C ↔ D) with four discrete spectral species [Figure 7B; (*30*)]. The

Table 3: Effect of Binding the MS Activation Domain to the FMN-Domain and MSR on the Midpoint Potentials of the FMN Cofactor in the FMN-Domain of MSR

	reduction potential (mV) vs normal hydrogen electrode			
	FMN		FAD	
	ox/sq	sq/hq	ox/sq	sq/hq
FMN-domain[a]	−94 ± 2	−192 ± 2		
FMN-domain[b]	−96 ± 2	−208 ± 20		
FMN-domain + Act-domain[a]	−86 ± 3	−170 ± 3		
FMN-domain + Act-domain[b]	−83 ± 3	−180 ± 28		
MSR[c]	−86 ± 1	−183 ± 1	−255 ± 5	−285 ± 4
MSR + Act-domain[c]	−85 ± 1	−185 ± 1	−275 ± 5	−322 ± 11
MSR[d]	−77 ± 2	−183 ± 2	−262 ± 23	−289 ± 14
MSR + Act-domain[d]	−81 ± 1	−178 ± 4	−221 ± 9	−308 ± 20

[a] Determined from nonlinear least-squares fit of the data at 600 nm shown in Figure 5A. [b] Determined from nonlinear least-squares fit of the data at 454 nm shown in Figure 5B. [c] Determined from nonlinear least-squares fit of the data isosbestic points (501 and 425 nm). [d] Determined from global analysis of data processed by SVD.

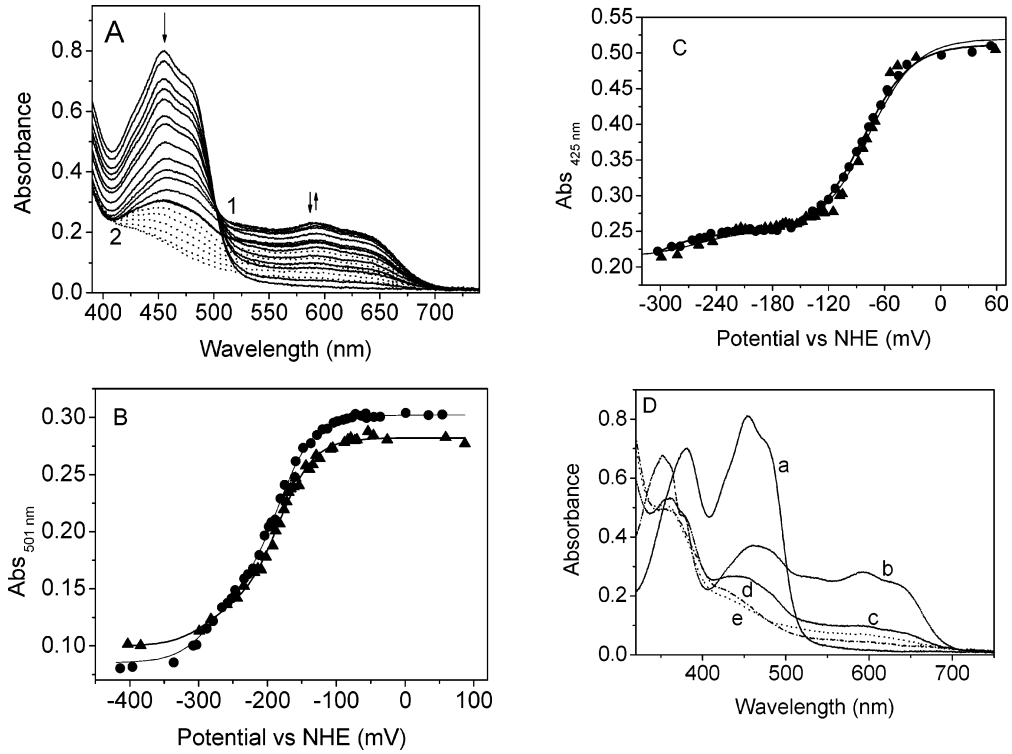

FIGURE 6: UV−visible absorption spectra collected during spectroelectrochemical titration of full-length MSR. MSR concentration is 31 μM. (Panel A) Arrows indicate direction of absorption change at key wavelengths during the reductive phase of the redox titrations. The solid lines demark spectra recorded during the addition of the first electron (i.e., conversion of the FMN oxidized to semiquinone state). An isosbestic point at 501 nm appearing during this transition is indicated by "1". The dashed lines indicate spectra recorded between approximately −140 and −240 mV. The dotted lines indicate spectra at potentials more negative than −240 mV, where an isosbestic point at 425 nm, denoted by "2", appears. (Panel B) Plot of absorbance at 425 nm with (▲) and without (●) the activation domain (40 μM) against potential. (Panel C) Plot of absorbance at 501 nm with (▲) and without (●) the activation domain (40 μM) against potential. The data were fitted to eq 7, as described in Experimental Procedures, and the midpoint potentials for all four couples are shown in Table 4. (Panel D) The deconvoluted spectra of *a*, oxidized; *b*, 1 electron-reduced; *c*, 2 electron-reduced; *d*, 3 electron-reduced; and *e*, 4 electron-reduced enzymes, determined by global analysis of the data in Panel A as described in Experimental Procedures. Experimental conditions: anaerobic titrations were performed in 50 mM Tris-HCl buffer at pH 7.5 and 25 °C.

spectral intermediates represent an equilibrium distribution of enzyme species that are formed in resolvable kinetic phases. Scheme 1 illustrates the reaction scheme we published previously for MSR alone showing what each intermediate might represent in terms of kinetically relevant enzyme intermediates (*30*). The rate constants of formation and decay of the spectral intermediates are shown in Table 4. Brackets are placed around the first $NADP^+$ shown in Scheme 1 because it is unclear if this molecule dissociates prior or subsequent to the formation of spectral species C (*30*).

The conversion of the fully oxidized enzyme (spectral species A) to the second intermediate (species B) occurs at 23.5 ± 0.1 s^{-1} and 25.5 ± 0.1 s^{-1} in the absence and presence of the activation domain, respectively. A 20% decrease in amplitude reflects 40% reduction of MSR to the two electron state in the first hydride transfer. The observed forward rate constants for the interconversion of spectral species B and C are 0.51 ± 0.02 s^{-1} for MSR alone and 0.41 ± 0.02 s^{-1} for MSR in the presence of the activation domain. Judging by the decrease in absorbance at 454 nm, the majority of the enzyme is reduced at the two-electron

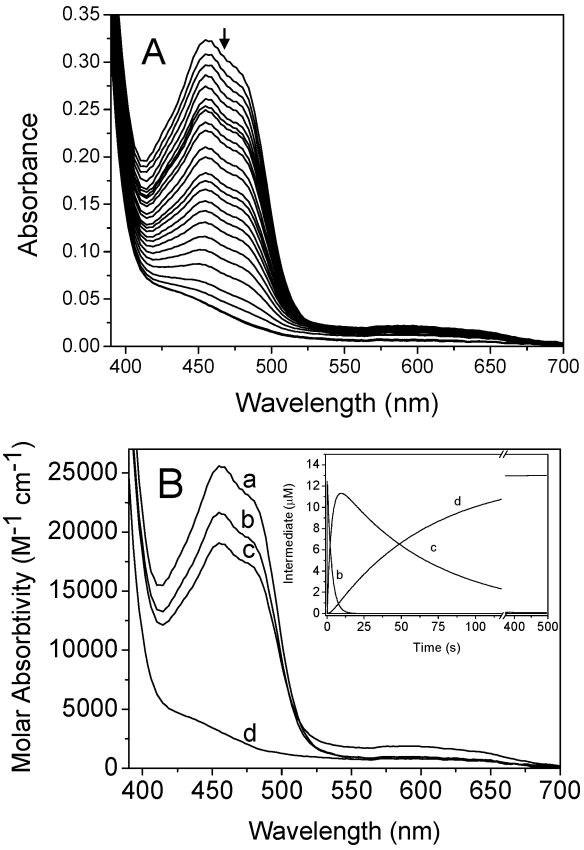

FIGURE 7: Reaction of human MSR with NADPH monitored by stopped-flow photodiode array spectroscopy. Conditions: 50 mM Tris-HCl at pH 7.5, 25 °C, 13 μM MSR concentration, 0.5 mM NADPH concentration. (Panel A) Time-dependent spectral changes occurring over 500 s following rapid mixing of MSR with NADPH. For clarity, only subsequent select spectra are shown. (Panel B) Deconvoluted spectra of the intermediates resolved from time-dependent SVD analysis of the data shown in panel A. The data shown in panel A were fitted globally to a three-step reversible model of A ↔ B ↔ C ↔ D. The observed rate constants obtained from the analysis are listed in Table 4. (Inset) Calculated concentration profiles (over 500 s) of intermediates in the reaction of MSR with NADPH. Profiles were obtained by fitting the data shown in panel A to a sequential reversible model of A ↔ B ↔ C ↔ D.

Scheme 1

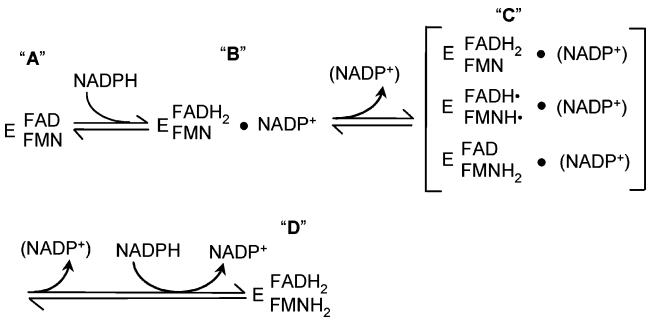

level at the completion of this kinetic phase. A small signature at 600 nm in spectral species C indicates that a population of the enzyme is in the disemiquinoid (FAD_{sq}/FMN_{sq}) state, in equilibrium with the FAD_{hq}/FMN_{ox} and/or FAD_{ox}/FMN_{hq} forms of MSR. The formation of MSR reduced at the level of four electrons occurs during the accumulation of spectral species D and is represented by further bleaching of absorbance at 454 and 600 nm. The formation of spectral species D occurs with rate constants of 0.015 ± 0.001 s^{-1} and 0.010 ± 0.001 s^{-1} in the presence and absence of the activation domain, respectively. Combined, these data indicate that the presence of the activation domain does not influence the kinetics of hydride transfer or interflavin electron transfer in MSR.

Table 4: Comparison of Kinetic Rate Constants for Electron Transfer in MSR in the Presence and Absence of the MS Activation Domain

	MSR (s^{-1})	MSR + Act-domain (s^{-1})
A → B	23.5 ± 0.1	25.5 ± 0.1
B → A	$(3.9 \pm 0.5) \times 10^{-5}$	$(3.0 \pm 0.5) \times 10^{-5}$
B → C	0.51 ± 0.02	0.41 ± 0.02
C → B	$(1.1 \pm 0.3) \times 10^{-6}$	$(6.1 \pm 0.1) \times 10^{-5}$
C → D	$1.5 \times 10^{-2} \pm 0.01 \times 10^{-3}$	$1.0 \times 10^{-2} \pm 0.01 \times 10^{-3}$
D → C	$(6.3 \pm 0.1) \times 10^{-6}$	$(1.5 \pm 0.8) \times 10^{-5}$

DISCUSSION

Most information on the structural and functional behavior of MS is derived from biochemical and biophysical studies of MetH. MetH, and by extension MS, are envisioned to be highly dynamic proteins as both substrate binding pockets on the N-terminal module [separated by 50 Å; (*31*)] and the activation domain (*32*) form discrete complexes with the cobalamin-binding domain to (i) catalyze each of the transmethylation reactions of the primary catalytic cycle and (ii) reactivate cob(II)alamin (*33*). There is an added level of complexity with the human system compared to that in *E. coli*, in that human MSR is also a multidomain protein.

The complexity imposed by the multidomain structure of MSR is (partially) removed by studying the properties of the individual flavin domains, which structurally and functionally mimic the properties of the corresponding domains in full-length MSR (*22*). With the isolated FMN-domain, we observe similarities between the human and *E. coli* reactivation systems. The dissociation constant (~1 μM) and binding stoichiometry (~1) for the complex formed between the activation domain and the FMN-domain are identical, within error, to the values reported for the binding of Fld to MetH (*20*). However, the thermodynamic parameters (i.e., change in enthalpy and entropy) associated with binding of human FMN-domain and activation domain are dissimilar to those reported for the *E. coli* counterparts, which were reported to be endothermic and entropically driven (*20*).

A potential difference in binding mode and/or affinity was hypothesized on the basis of a superposition of the crystal structures for human MS and *E. coli* MetH activation domains (Figure 8). The structural overlay reveals that Lys959 and Lys1035 of MetH (both known to be important residues in the binding interface with Fld) are located ~25 and ~7 Å, respectively, from the corresponding residues in human MS, Lys987 and Lys1071[2]. Despite this structural difference between the two proteins, Lys987 and Lys1071 form part of the protein interface in complex with MSR because neutralization of these residues (by mutation to threonine) resulted in a decrease in binding affinity, similar to that observed for the corresponding mutations (K1035T and K959T) in MetH (*20*). This functional equivalence of interface residues between the human and MetH systems is

[2] The published crystal structure of the human MS activation domain contains two amino acid changes (D963E and K1071N) from that of the published sequence (Genbank accession number: Q99707).

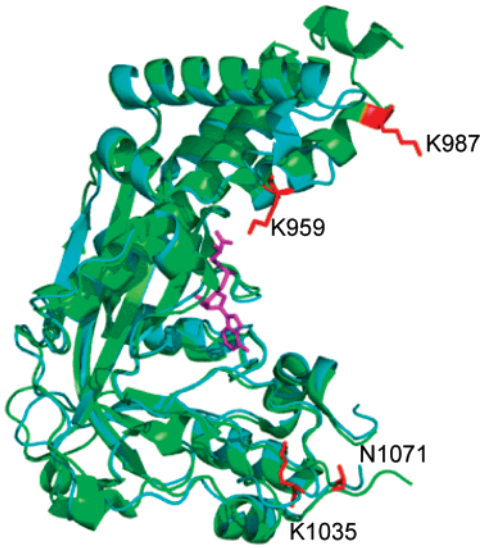

FIGURE 8: Superposition of the human MS and *E. coli* MetH activation domains. The *E. coli* and human proteins are shown in blue and green, respectively. AdoMet from the *E. coli* structure [1MSK, (*18*)] is denoted in stick representation (magenta). Asn1071 and Lys959 of human MS, and Lys1035 and Lys959 of MetH are shown as red sticks.

not retained for at least one residue located on the surface of the FMN-binding domain of MSR. From our solution studies, we infer that residue Asp64 of the human FMN-domain does not form a salt bridge with human activation domain, which contrasts with the role of the counterpart residue (Glu61) in *E. coli* Fld.

We have demonstrated that the MSR−activation domain complex is less stable than the FMN-domain−activation domain complex. We also find a notable difference in the binding stoichiometry between these two complexes. Moreover, the binding of MSR to the activation domain is more endothermic and entropy driven compared with the complex formed with the FMN-domain. This might suggest that additional conformational changes and/or water movement is required for complex formation. The changed stoichiometry of the interaction with full-length MSR also suggests additional interactions. Given that the activation domain has a low propensity to dimerize in free solution (*19*), it is reasonable to suggest that the binding of MSR is to a dimeric form of the activation domain and that the monomer−dimer equilibrium for the activation is pulled toward the dimer structure in the ITC analysis. The structural implications of this stoichiometry need to be explored using crystallographic methods, but one might infer a role for the FAD/NADPH-binding domain and/or the connecting hinge domain in facilitating this protein interaction.

Olteanu and Banerjee have shown (under buffering conditions different from those employed in our study) that reactivation of MS *in vitro* requires a 4:1 ratio of MSR to MS for maximal activity (*3*). This contrasts with the 1:1 ratio of Fld to MetH required for the reactivation of MetH by *E. coli* Fld (*3*). The apparent dissociation constant is also higher for the MSR−MS complex (~80 nM) compared to that of the Fld−MetH complex [~5 nM; (*3*)], pointing to a weaker binding interaction between the partner proteins in the human complex. ITC binding isotherms and fluorescence binding assays reveal that the apparent binding constants are similar (at least for the MSR−FMN-domain interaction) to that of

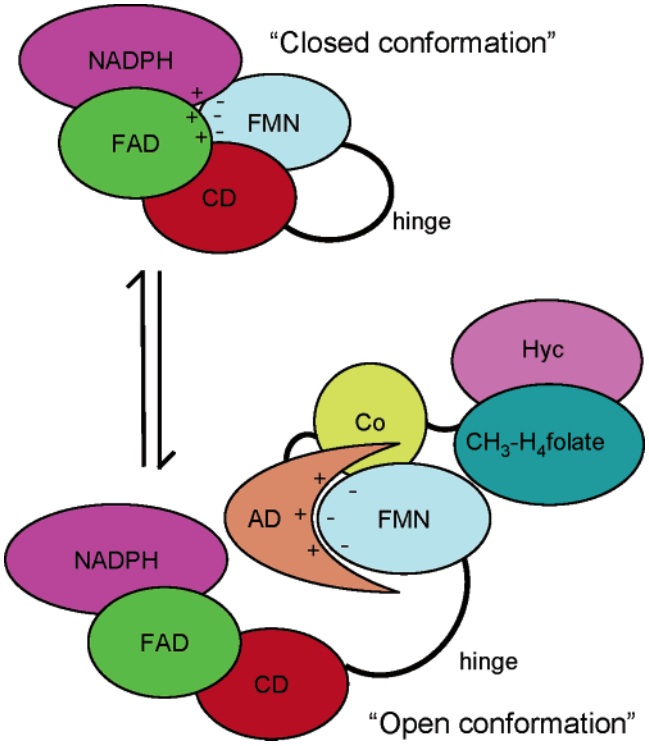

FIGURE 9: Model demonstrating the open and closed conformations of MSR. In the closed conformation, the FMN-domain is docked with the FNR-like module of MSR in a position that allows interflavin electron transfer. In the open conformation, the FMN domain has moved away from the rest of the MSR polypeptide and is in a conformation suitable for interaction with MS. Electrostatic interactions, denoted by + and − symbols, are thought to be important in the binding interface between the FMN-domain and the FNR-like module and also the activation domain. CD refers to the connecting domain of MSR, whereas Hyc, CH_3-H_4folate, and Co represent the homocysteine, CH_3-H_4folate, cobalamin-binding domains, respectively. AD is the activation domain.

the *E. coli* MetH system. This suggests a different interaction mode in the human FMN-domain−MS and MSR−MS complexes, with the FMN-domain−MS complex more closely mimicking the Fld−MetH complex.

The multidomain nature of MSR suggests a degree of conformational flexibility larger than that available in the *E. coli* system. By analogy with other diflavin oxidoreductases such as NOS (*17*), MSR may fluctuate between a closed and open conformation, that is, in one conformation (an open conformation) the FMN-domain is amenable for interaction with MS, and in another conformation (closed conformation) the FMN-domain is in close proximity to NADPH/FAD-binding domain (Figure 9). The multiple conformations would optimize electronic coupling to the FAD domain (closed conformation) and cob(II)alamin (open conformation) and require a swinging motion for the FMN-domain between the two states. Such a mechanism for electron transfer is in stark contrast to that observed in the Fld−MetH system (where Fld binds in a mutually exclusive manner to MetH or FNR and essentially as rigid body entities for the flavoprotein component; (*20*)) but more akin to models of electron transfer proposed for multidomain flavoprotein systems, such as CPR, NOS, and bacterial diflavin reductases (*15*), supporting the concept of large-scale conformational sampling proposed generally for multidomain electron transfer complexes (*34*−*36*). In the context of this model, we note that internal electron transfer in MSR is substantially

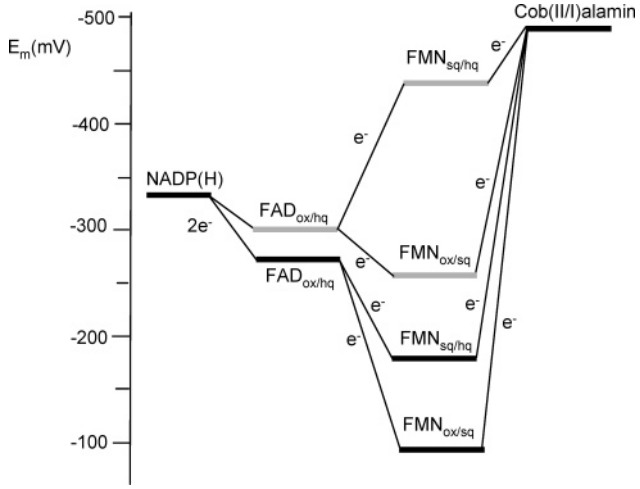

FIGURE 10: Scheme comparing the thermodynamics of electron transfer between MSR and MS, and between *E. coli* Fld and MetH. The midpoint potential values of FNR ($FAD_{ox/hq}$) and Fld ($FMN_{ox/sq}$ and $FMN_{sq/hq}$) are represented by gray lines, and the flavin couples of MSR are represented by black lines as is the cob(I)alamin/cob(II)alamin couple. Electron transfer from NADPH → FAD → FMN in MSR follows a customary downhill path as electrons are shuttled to redox centers that are progressively more electropositive. However, a significant uphill step is encountered with electron transfer from MSR to MS, as the midpoint potential of the cob(II)alamin/cob(I)alamin couple is substantially more electronegative than the MSR $FMN_{ox/sq}$ and $FMN_{sq/hq}$ couples. Electron transfer in the *E. coli* Fld−MetH complex is more thermodynamically feasible, as the corresponding values for the FMN midpoint potentials in Fld are more electronegative. The values cited are from the following refs: *5*, *22*, and *23*.

slower (>10-fold) than that observed in CPR (*37*) and NOS (*38*). Thermodynamically, internal electron transfer is favorable, and intrinsic rates of electron transfer are expected to be fast over physiologically sustainable distances (*39*). The observed slow rates for internal electron in MSR (as in CPR and NOS) imply some other form of control, either ligand gating (e.g., release of $NADP^+$) or conformational control through sampling mechanisms.

Electron transfer from MSR to cob(II)alamin presents a major thermodynamic obstacle (Figure 10). The midpoint potentials of the $FMN_{ox/sq}$ and $FMN_{sq/hq}$ are substantially more electropositive ($\Delta E = 170$ and 260 mV, respectively) than that of the cob(II)alamin/cob(I)alamin couple (*23*), translating, respectively, to a change in free energy of 16 kJ/mol and 25 kJ/mol. This contrasts with the situation with NOS and CPR in which electron transfer to their native electron acceptors is thermodynamically feasible. In CaM-free NOS, the $FMN_{ox/sq}$ couple is significantly more electropositive than the heme, but recent studies have shown that the binding of Ca^{2+}-activated CaM lowers the $FMN_{ox/sq}$ and $FMN_{sq/hq}$ couples to make the final step of electron transfer (from $FMNH_2$ at least) to the heme almost isopotential (*40*). In CPR, the $FMN_{ox/sq}$ couple has a higher midpoint potential than the P450 heme; however, the air stable FMN semiquinone does not serve as a reductant in the catalytic cycle (*41*), and the $FMN_{sq/hq}$ couple (−280 mV) is similar to that of the P450 heme (−300 mV). Also, the binding of type 1 substrates to the ferriheme raises the midpoint potential to make electron transfer more thermodynamically favorable (*42*). On the basis of the precedence for factors influencing the midpoint potential of NOS and CPR, we sought to determine whether the binding of the activation domain affects the thermodynamic properties of the flavins in MSR or the isolated FMN-domain. Our studies show that protein−protein interaction, at least with the activation domain of MS, does not significantly perturb the potentials of the four flavin couples, indicating that electron transfer to cob(II)alamin remains a highly endergonic process. Likewise, the binding of MetH to Fld does not significantly alter the midpoint potentials of the FMN cofactor, but the thermodynamic barrier is not so great in the *E. coli* system. Although the $FMN_{sq/hq}$ couple is nearly isopotential with the cob(II)alamin/cob(I)alamin couple, it is thought that the FMN semiquinone is the primary electron donor because under aerobic growth, the potential of the cell (E_{cell}) is −330 mV [thus favoring the one electron reduced form of the cofactor; (*5*)]. The resulting uphill electron transfer from FMN semiquinone to cob(II)alamin ($\Delta E \approx +230$ mV) is thought to be coupled to irreversible methyl transfer from AdoMet, a highly exothermic reaction [$\Delta H^\circ = -55$ kJ/mol; (*43*)]. We suggest that the driving force for reductive methylation of human MS is also tightly coupled to methyl group transfer from AdoMet. It is worth noting that, until relatively recently, the paradigm for biological electron transfer has assumed that electrons should flow energetically downhill through redox centers that become progressively more electropositive (as is the case with MSR in catalyzing electron transfer from NADPH to FAD to FMN; Figure 10). However, unfavorable electron tunneling steps are observed in natural electron transfer proteins such as hydrogenase (*44*), nitrate reductase (*44*), and membrane-bound respiratory chains (*45*). In those cases where an endergonic electron transfer step has been engineered (e.g., methylamine dehydrogenase), electron tunneling still occurs, albeit at a substantially slower but functionally relevant rate (*46*). Dutton and co-workers have shown that the close proximity (<6 Å) of redox centers alone is sufficient to allow endergonic electron transfer at a rate that is catalytically and physiologically relevant (*39*). In the absence of obvious modulators of the MSR reduction potentials, a conformational sampling mechanism for MSR in which the FMN-domain approaches the cob(II)alamin cofactor in the MS−MSR complex, linked to a highly exothermic methyl transfer step, is likely sufficient to ensure endergonic electron transfer between that the FMN and cob(II)alamin redox centers.

CONCLUDING REMARKS

The 1:2 stoichiometry of the MSR−MS complex is consistent with the presence of an activation dimer in the complex. Cross-linking and mutagenesis studies indicate some conservation of interacting residues in the *E. coli* and human reactivation complexes but also highlight significant differences. Electron transfer in MSR is neither thermodynamically nor kinetically modulated by association with the activation domain of human MS. Electron transfer to cob(II)alamin is substantially endergonic in human MS−MSR, suggesting an endergonic tunneling step linked to an exothermic methyl group transfer.

SUPPORTING INFORMATION AVAILABLE

Comparison of the electrostatic potentials of the surface of *E. coli* Fld and of a model of the FMN domain of human

MSR (Figure S1). This material is available free of charge via the Internet at http://pubs.acs.org.

NOTE ADDED AFTER ASAP PUBLICATION

This paper was published ASAP 05/04/07. Reference 40 has been updated; the corrected version was published 05/11/07.

REFERENCES

1. Matthews, R. G. (2001) Cobalamin-dependent methyltransferases, *Acc. Chem. Res. 34*, 681−689.
2. Drummond, J. T., Huang, S., Blumenthal, R. M., and Matthews, R. G. (1993) Assignment of enzymatic function to specific protein regions of cobalamin-dependent methionine synthase from *Escherichia coli*, *Biochemistry 32*, 9290−9295.
3. Olteanu, H., and Banerjee, R. (2001) Human methionine synthase reductase, a soluble P-450 reductase-like dual flavoprotein, is sufficient for NADPH-dependent methionine synthase activation, *J. Biol. Chem. 276*, 35558−35563.
4. Leclerc, D., Odievre, M., Wu, Q., Wilson, A., Huizenga, J. J., Rozen, R., Scherer, S. W., and Gravel, R. A. (1999) Molecular cloning, expression and physical mapping of the human methionine synthase reductase gene, *Gene 240*, 75−88.
5. Jarrett, J. T., Hoover, D. M., Ludwig, M. L., and Matthews, R. G. (1998) The mechanism of adenosylmethionine-dependent activation of methionine synthase: a rapid kinetic analysis of intermediates in reductive methylation of Cob(II)alamin enzyme, *Biochemistry 37*, 12649−12658.
6. Fujii, K., Galivan, J. H., and Huennekens, F. M. (1977) Activation of methionine synthase: further characterization of flavoprotein system, *Arch. Biochem. Biophys. 178*, 662−670.
7. Jarrett, J. T., Huang, S., and Matthews, R. G. (1998) Methionine synthase exists in two distinct conformations that differ in reactivity toward methyltetrahydrofolate, adenosylmethionine, and flavodoxin, *Biochemistry 37*, 5372−5382.
8. Chou, Y. C., Lee, M. S., Wu, M. H., Shih, H. L., Yang, T., Yu, C. P., Yu, J. C., and Sun, C. A. (2006) Plasma homocysteine as a metabolic risk factor for breast cancer: findings from a case-control study in Taiwan, *Breast Cancer Res. Treat. 101*, 199−205.
9. Ma, J., Stampfer, M. J., Christensen, B., Giovannucci, E., Hunter, D. J., Chen, J., Willett, W. C., Selhub, J., Hennekens, C. H., Gravel, R., and Rozen, R. (1999) A polymorphism of the methionine synthase gene: association with plasma folate, vitamin B12, homocyst(e)ine, and colorectal cancer risk, *Cancer Epidemiol., Biomarkers Prev. 8*, 825−829.
10. Jacques, P. F., Bostom, A. G., Selhub, J., Rich, S., Ellison, R. C., Eckfeldt, J. H., Gravel, R. A., and Rozen, R. (2003) Effects of polymorphisms of methionine synthase and methionine synthase reductase on total plasma homocysteine in the NHLBI family heart study, *Atherosclerosis 166*, 49−55.
11. Wilson, A., Leclerc, D., Rosenblatt, D. S., and Gravel, R. A. (1999) Molecular basis for methionine synthase reductase deficiency in patients belonging to the cblE complementation group of disorders in folate/cobalamin metabolism, *Hum. Mol. Genet. 8*, 2009−2016.
12. Stuehr, D. J., Cho, H. J., Kwon, N. S., Weise, M. F., and Nathan, C. F. (1991) Purification and characterization of the cytokine-induced macrophage nitric oxide synthase: an FAD- and FMN-containing flavoprotein, *Proc. Natl. Acad. Sci. U.S.A. 88*, 7773−7777.
13. Bredt, D. S., Hwang, P. M., Glatt, C. E., Lowenstein, C., Reed, R. R., and Snyder, S. H. (1991) Cloned and expressed nitric oxide synthase structurally resembles cytochrome P-450 reductase, *Nature 351*, 714−718.
14. Paine, M. J., Garner, A. P., Powell, D., Sibbald, J., Sales, M., Pratt, N., Smith, T., Tew, D. G., and Wolf, C. R. (2000) Cloning and characterization of a novel human dual flavin reductase, *J. Biol. Chem. 275*, 1471−1478.
15. Wang, M., Roberts, D. L., Paschke, R., Shea, T. M., Masters, B. S., and Kim, J. J. (1997) Three-dimensional structure of NADPH-cytochrome P450 reductase: prototype for FMN- and FAD-containing enzymes, *Proc. Natl. Acad. Sci. U.S.A. 94*, 8411−8416.
16. Hall, D. A., Vander Kooi, C. W., Stasik, C. N., Stevens, S. Y., Zuiderweg, E. R., and Matthews, R. G. (2001) Mapping the interactions between flavodoxin and its physiological partners flavodoxin reductase and cobalamin-dependent methionine synthase, *Proc. Natl. Acad. Sci. U.S.A. 98*, 9521−9526.
17. Garcin, E. D., Bruns, C. M., Lloyd, S. J., Hosfield, D. J., Tiso, M., Gachhui, R., Stuehr, D. J., Tainer, J. A., and Getzoff, E. D. (2004) Structural basis for isozyme-specific regulation of electron transfer in nitric-oxide synthase, *J. Biol. Chem. 279*, 37918−37927.
18. Dixon, M. M., Huang, S., Matthews, R. G., and Ludwig, M. (1996) The structure of the C-terminal domain of methionine synthase: presenting S-adenosylmethionine for reductive methylation of B12, *Structure 4*, 1263−1275.
19. Wolthers, K. R., Toogood, H. S., Jowitt, T. A., Marshall, K. R., Leys, D., and Scrutton, N. S. (2007) Crystal structure and solution characterization of the activation domain of human methionine synthase, *FEBS J. 274*, 738−750.
20. Hall, D. A., Jordan-Starck, T. C., Loo, R. O., Ludwig, M. L., and Matthews, R. G. (2000) Interaction of flavodoxin with cobalamin-dependent methionine synthase, *Biochemistry 39*, 10711−10719.
21. Yamada, K., Gravel, R. A., Toraya, T., and Matthews, R. G. (2006) Human methionine synthase reductase is a molecular chaperone for human methionine synthase, *Proc. Natl. Acad. Sci. U.S.A. 103*, 9476−9481.
22. Wolthers, K. R., Basran, J., Munro, A. W., and Scrutton, N. S. (2003) Molecular dissection of human methionine synthase reductase: determination of the flavin redox potentials in full-length enzyme and isolated flavin-binding domains, *Biochemistry 42*, 3911−3920.
23. Hoover, D. M., Jarrett, J. T., Sands, R. H., Dunham, W. R., Ludwig, M. L., and Matthews, R. G. (1997) Interaction of *Escherichia coli* cobalamin-dependent methionine synthase and its physiological partner flavodoxin: binding of flavodoxin leads to axial ligand dissociation from the cobalamin cofactor, *Biochemistry 36*, 127−138.
24. Sancho, J. (2006) Flavodoxins: sequence, folding, binding, function and beyond, *Cell. Mol. Life Sci. 63*, 855−864.
25. Hoover, D. M., and Ludwig, M. L. (1997) A flavodoxin that is required for enzyme activation: the structure of oxidized flavodoxin from *Escherichia coli* at 1.8 Å resolution, *Protein Sci. 6*, 2525−2537.
26. Brown, C. A., McKinney, K. Q., Kaufman, J. S., Gravel, R. A., and Rozen, R. (2000) A common polymorphism in methionine synthase reductase increases risk of premature coronary artery disease, *J. Cardiovasc. Risk 7*, 197−200.
27. Wilson, A., Platt, R., Wu, Q., Leclerc, D., Christensen, B., Yang, H., Gravel, R. A., and Rozen, R. (1999) A common variant in methionine synthase reductase combined with low cobalamin (vitamin B12) increases risk for spina bifida, *Mol. Genet. Metab. 67*, 317−323.
28. Olteanu, H., Munson, T., and Banerjee, R. (2002) Differences in the efficiency of reductive activation of methionine synthase and exogenous electron acceptors between the common polymorphic variants of human methionine synthase reductase, *Biochemistry 41*, 13378−13385.
29. Olteanu, H., Wolthers, K. R., Munro, A. W., Scrutton, N. S., and Banerjee, R. (2004) Kinetic and thermodynamic characterization of the common polymorphic variants of human methionine synthase reductase, *Biochemistry 43*, 1988−1997.
30. Wolthers, K. R., and Scrutton, N. S. (2004) Electron transfer in human methionine synthase reductase studied by stopped-flow spectrophotometry, *Biochemistry 43*, 490−500.
31. Evans, J. C., Huddler, D. P., Hilgers, M. T., Romanchuk, G., Matthews, R. G., and Ludwig, M. L. (2004) Structures of the N-terminal modules imply large domain motions during catalysis by methionine synthase, *Proc. Natl. Acad. Sci. U.S.A. 101*, 3729−3736.
32. Bandarian, V., Pattridge, K. A., Lennon, B. W., Huddler, D. P., Matthews, R. G., and Ludwig, M. L. (2002) Domain alternation switches B(12)-dependent methionine synthase to the activation conformation, *Nat. Struct. Biol. 9*, 53−56.
33. Bandarian, V., Ludwig, M. L., and Matthews, R. G. (2003) Factors modulating conformational equilibria in large modular proteins: a case study with cobalamin-dependent methionine synthase, *Proc. Natl. Acad. Sci. U.S.A. 100*, 8156−8163.
34. Toogood, H. S., van Thiel, A., Basran, J., Sutcliffe, M. J., Scrutton, N. S., and Leys, D. (2004) Extensive domain motion and electron transfer in the human electron transferring flavoprotein·medium chain Acyl-CoA dehydrogenase complex, *J. Biol. Chem. 279*, 32904−32912.

35. Leys, D., Basran, J., Talfournier, F., Sutcliffe, M. J., and Scrutton, N. S. (2003) Extensive conformational sampling in a ternary electron transfer complex, *Nat. Struct. Biol. 10*, 219−225.
36. Toogood, H. S., van Thiel, A., Scrutton, N. S., and Leys, D. (2005) Stabilization of non-productive conformations underpins rapid electron transfer to electron-transferring flavoprotein, *J. Biol. Chem. 280*, 30361−30366.
37. Gutierrez, A., Lian, L. Y., Wolf, C. R., Scrutton, N. S., and Roberts, G. C. (2001) Stopped-flow kinetic studies of flavin reduction in human cytochrome P450 reductase and its component domains, *Biochemistry 40*, 1964−1975.
38. Knight, K., and Scrutton, N. S. (2002) Stopped-flow kinetic studies of electron transfer in the reductase domain of neuronal nitric oxide synthase: re-evaluation of the kinetic mechanism reveals new enzyme intermediates and variation with cytochrome P450 reductase, *Biochem. J. 367*, 19−30.
39. Page, C. C., Moser, C. C., Chen, X., and Dutton, P. L. (1999) Natural engineering principles of electron tunnelling in biological oxidation-reduction, *Nature 402*, 47−52.
40. Dunford, A. J., Rigby, S. E. J., Hay, S., Munro, A. W., Scrutton, N. S. (2007) Conformational and Thermodynamic Control of Electron Transfer in Neuronal Nitric Oxide Synthase, *Biochemistry 46* (17), 5018−5029.
41. Munro, A. W., Noble, M. A., Robledo, L., Daff, S. N., and Chapman, S. K. (2001) Determination of the redox properties of human NADPH-cytochrome P450 reductase, *Biochemistry 40*, 1956−1963.
42. Sligar, S. G., Cinti, D. L., Gibson, G. G., and Schenkman, J. B. (1979) Spin state control of the hepatic cytochrome P450 redox potential, *Biochem. Biophys. Res. Commun. 90*, 925−932.
43. Mudd, S. H., Klee, W. A., and Ross, P. D. (1966) Enthalpy changes accompanying the transfer of a methyl group from S-adenosyl methionine and other sulfonium compounds to homocysteine, *Biochemistry 5*, 1653−1660.
44. Rousset, M., Montet, Y., Guigliarelli, B., Forget, N., Asso, M., Bertrand, P., Fontecilla-Camps, J. C., and Hatchikian, E. C. (1998) [3Fe-4S] to [4Fe-4S] cluster conversion in *Desulfovibrio fructosovorans* [NiFe] hydrogenase by site-directed mutagenesis, *Proc. Natl. Acad. Sci. U.S.A. 95*, 11625−11630.
45. Chen, I. P., Mathis, P., Koepke, J., and Michel, H. (2000) Uphill electron transfer in the tetraheme cytochrome subunit of the *Rhodopseudomonas viridis* photosynthetic reaction center: evidence from site-directed mutagenesis, *Biochemistry 39*, 3592−3602.
46. Sun, L. J., Yim, C. K., and Verdine, G. L. (2001) Chemical communication across the zinc tetrathiolate cluster in *Escherichia coli* Ada, a metalloactivated DNA repair protein, *Biochemistry 40*, 11596−11603.

BI700339V